The Effect Of Detachment On Carbon Divertor Erosion/Redeposition in the DIII-D Tokamak

D.G. Whyte[1*], W.P. West[2], C.P.C. Wong[2], R. Bastasz[3], J.N. Brooks[4], W.R. Wampler[3], N.H. Brooks[2], J.W. Davis[5], R.P. Doerner[1], A.A. Haasz[5], R.C. Isler[6], G.L. Jackson[2], R.G. Macaulay-Newcombe[5], M.R. Wade[6]
1) Fusion Energy Research Program, University of California, San Diego, California USA
2) General Atomics, P.O. Box 85608, San Diego, California 92186-5608 USA
3) Sandia National Laboratories, Albuquerque, New Mexico & Livermore, California USA
4) Argonne National Laboratory, Argonne, Illinois USA
5) University of Toronto Institute for Aerospace Studies, Toronto, Canada
6) Oak Ridge National Laboratory, Oak Ridge, Tennessee USA
*e-mail contact of corresponding author: dwhyte@ucsd.edu

Abstract. The DIII-D tokamak has demonstrated an operational scenario where the graphite-covered divertor is free of net erosion. Reduction of divertor carbon erosion is accomplished using a low temperature (detached) divertor plasma that eliminates physical sputtering. Likewise, the carbon source rate arising from chemical erosion is found to be very low in the detached divertor. Near strikepoint regions, the rate of carbon deposition is ~3 cm/burn-year, with a corresponding hydrogenic codeposition rate > 1 kg/m^2/burn-year; rates both problematic for steady-state fusion reactors. The carbon net deposition rate in the divertor is consistent with carbon arriving from the core plasma region. Carbon influx from the main wall is measured to be relatively large in the high-density detached regime and is of sufficient magnitude to account for the deposition rate in the divertor. Divertor redeposition is therefore determined by non-divertor erosion and transport. Despite the success in reducing divertor erosion on DIII-D with detachment, no significant reduction is found in the core plasma carbon density, illustrating the importance of non-divertor erosion and the complex coupling between erosion/redeposition and impurity plasma transport.

1. Introduction

Methods must be developed to control both the erosion/redeposition (E/R) of plasma-facing materials and the heat flux to divertor components in the next generation of tokamaks that will operate with long pulses or at steady-state (i.e. next-step devices). Two related yet distinct problems arise for E/R in Next-Step devices; namely limited component lifetime due to net erosion, and the trapping of tritium fuel in redeposited layers. E/R does not cause serious operational problems in current tokamaks because of the very low operational duty-cycle. Nevertheless, the magnitude, cause and possible solution to E/R issues is being addressed scientifically to ensure operational viability of future tokamaks. The operational regime commonly referred to as detachment has been demonstrated on current tokamaks to reduce divertor heat flux [1]. Detachment is characterized by a high density, cold plasma (electron temperature $T_e < 2$ eV) near divertor strikepoints. The use of detachment will likely be a necessary ingredient in any burning tokamak that uses a poloidal divertor geometry (see for example ITER design [2]). Detachment will simultaneously have strong effects on plasma-material interactions (PMI), and therefore E/R. The low electron temperature associated with detachment reduces the energy of bombarding ions, and therefore reduces or eliminates the ability of the ions to remove material through physical sputtering. Furthermore, the high density, cold plasma affects ionization (i.e. opacity) and transport of sputtered atoms and molecules through the divertor plasma. It seems necessary then to understand plasma-material interactions and E/R in the detached regime, and if possible, develop scenarios of detachment that additionally optimize control of E/R. DIII-D is well suited for this task for several reasons. First, a set of material sample exposures (Divertor Material Evaluation System, DiMES [3]) has furnished a "map" of the divertor E/R for a specific detached plasma condition. Second, the open lower divertor is well diagnosed for both the plasma and PMI. Third, carbon is the primary plasma-facing material in DIII-D and will likely be the initial choice of divertor material in a next-step tokamak due to its resilience to transient heating [2].

2. Experimental Erosion/Redeposition Results

E/R experiments are performed with lower single-null magnetic geometry. The open lower divertor of DIII-D has a large array of plasma and surface diagnostics. A material sample

probe (DiMES [3]) can be inserted and retracted from the horizontal lower divertor target plates.

Previous E/R measurements [3-5] show that "attached" tokamak plasma operation of a single-null divertor leads to the following scenario: net erosion occurs near the outer strikepoint (OSP) region, while net deposition occurs at the inner strikepoint (ISP) region (Fig. 1). In this case, the outer divertor is an ionizing, hot (T_e> 10 eV) plasma, with a sharply peaked heat flux profile and a typical peak heat flux of 1-5 MW m^{-2} (Fig. 2). The inner divertor leg plasma is colder with regions of significant plasma volume recombination [6]. The rate of net erosion is >10 cm/ burn-year (1nm/s ~ 3 cm /burn-year) in a narrow region near the OSP. Hydrogenic trapping is higher than 1 kg/m^2/burn-year in the inner divertor region [4]. Good agreement to the measured carbon sputtering and net erosion is obtained from modeling [7] which uses the measured OSP plasma and exposure conditions. The modeling shows that physical sputtering of carbon by both deuterium and carbon (i.e. self-sputtering) and near-surface ionization and transport of sputtered carbon is the cause of high net erosion near the OSP. The effective sputtering yield (ratio of sputtered carbon flux to incident plasma flux) can be as high as 10% at the OSP for deuterium plasmas on graphite.

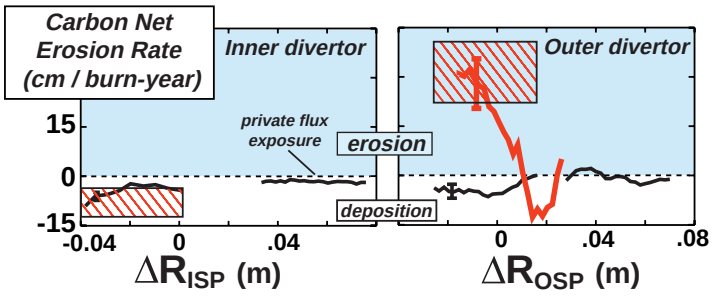

Fig. 1 Summary of carbon E/R rates in DIII-D lower divertor for attached (red) and detached (black) divertor. Hatched areas from height measurements on DIII-D tiles exposed for 9 months [3]. *Net redeposition is plotted as negative net erosion.*

Detachment of the outer divertor leg is used to control net carbon erosion. For these experiments, OSP detachment is obtained by controlled deuterium injection with no active pumping. The line-averaged density increases and confinement remains at H-mode level but is somewhat degraded (H_{L89} ~ 1.5). Injected neutral beam heating power is 7 MW. The plasma continues ELMing, with the ELMs becoming more frequent. Thomson scattering shows that outer divertor detachment is characterized by a cold plasma at the divertor plate with T_e~1.5 eV. The divertor plasma temperature becomes very uniform across the entire divertor plate (Fig. 2). This low electron temperature eliminates physical sputtering for impinging ions on the divertor plate. The plate ion flux generally *increases* across the outer divertor leg and peaks ~0.1 m outboard of the OSP. Divertor electron density is high, n_e >10^{20} m^{-3}, as well as the neutral/molecular density (P> 10^{-2} Torr). Energy balance and Mach probe measurements find that the parallel plasma flow is near the sound speed (M~0.75 [8]) and flowing toward the plates in both divertor legs. DiMES graphite probes were used to measure the E/R pattern in this detached case. The plasma geometry was altered from exposure-to-exposure to allow erosion measurements at different magnetic locations with the fixed-position DiMES probe [9]. The DiMES probe results show that net carbon erosion is eliminated across the divertor floor (Fig. 1). Carbon net deposition rates vary across the divertor floor, being highest near the strikepoints (~3-5 cm/burn-year) and lowest at the private-flux (PF) and outer SOL (≤ 1 cm/burn-year). A region of zero net E/R (within the uncertainties) is located in the outer strike zone close to the peak

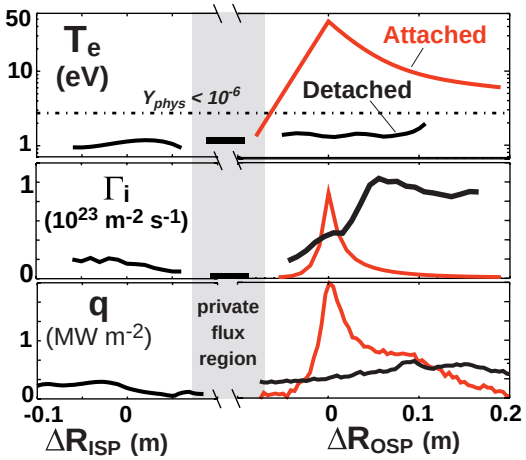

Fig. 2 Comparison of divertor plate plasma parameters in attached (red) and detached (black) states for E/R measurements case shown in Fig. 1.

in ion flux. Significant deposition occurs at the PF divertor plate despite very low incident plasma flux at this location.

3. Carbon Sources And Transport In Detached Plasmas

Visible spectroscopy shows significant C I (atomic carbon) emission from the divertor region, yet at the divertor strike plates the plasma temperature is well below the threshold for physical sputtering of graphite. The cold plasma region extends from the divertor strike plates up along the divertor legs to a vertical height about equal to the X-point. In this cold region the neutral C I has a long mean free path and a very low excitation rate, and as a result is essentially invisible to spectroscopy. Thus we expect that the C I (and CII) emission is produced in the ionization front above the strike plate where the plasma electron temperature increases to >5 eV [6]. There are four possible sources of the C I emission. First, carbon is physically sputtered during ELMs. Second, chemically eroded hydrocarbon molecules from the strike plates dissociate to the atomic state. Third, carbon ions from the hot core and scrape off layer (SOL) transport into the cold dense plasma and recombine to the neutral state. Fourth, carbon erosion occurs at the divertor "throat", away from strikepoints and penetrates to the ionization front. In the following analysis we will show that the first two sources are unimportant, indicating that non divertor regions are the major source of carbon.

Although the quiescent plasma is too cold to physically sputter carbon, sputtering during short duration (~ 1 ms) ELMs might provide a source of C I emission, which would appear close to the plate (carbon atom transport times << ionization time). Zeeman splitting measurements of C I have been used to verify that the time-averaged C I emission is indeed localized to a region >0.1 m above the divertor plate during detachment (Fig. 3). Therefore, physical sputtering of carbon during ELMs is unimportant in the time-averaged sense.

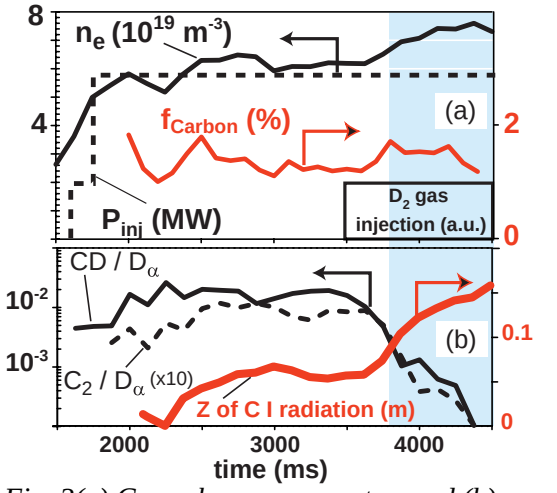

Fig. 3(a) Core plasma parameter, and (b) chemical erosion emissions and vertical location, Z, from divertor floor of CI radiation during transition to detachment (shaded region).

Carbon might also be sputtered at the divertor strike plates by chemical processes, producing volatile hydrocarbons (e.g. CD_4, C_2D_4, etc.) that are dissociated by the plasma, finally producing atomic carbon. Chemical sputtering has a much lower energy threshold than physical sputtering [10]. The diagnostic tool used to measure chemical erosion is the visible emissions of hydrocarbon radical states (CD and C_2) produced by plasma dissociation and excitation. Unlike carbon atoms and ions, these radical species can ionize through charge-exchange (Fig. 4) and radiate in the cold detached plasmas (via direct excitation from the molecular ground state). CD and C_2 intensities normalized to incident flux (D_α) are seen to decrease significantly through detachment (Fig. 3). Yet, the photon efficiency for relating CD emission to CD influx [11,12] *increases* in detachment. Fig. 5 shows the CD particle flux (~ 1.5×10^{19} $m^{-2}s^{-1}$) is much smaller than the C I flux (~8×10^{20} $m^{-2}s^{-1}$) at the ionization front, indicating that chemical erosion cannot be a significant contributor to C I emission. The possibility that non-methane species are instead dominating chemical erosion is likely ruled out by the similar behavior of the C_2 emissions through detachment. The inferred chemical erosion yield using available photon efficiencies [13,14], Y_{chem}~ 0.01-0.02%, is very low compared to Y_{chem}~1% and Y_{total} > 5% for the attached case. However, this result is inconsistent with a study of ion beam induced chemical erosion of a tile removed from DIII-D [5,15] that exhibits Y_{chem}~ 1 %. It is possible, but unverified, that the chemical yield is much larger than the 0.01% derived from the spectroscopic data, but the hydrocarbons are quickly ionized and redeposited before they have a chance to radiate. In practice, though, such very prompt redeposition has the same effect as very low yield in terms of carbon sources.

The C I emission can arise from carbon ions from the hot core and scrape off layer (SOL) transporting into the cold dense plasma and recombining to the neutral state. Fig. 4 shows the details of measurements and calculations along the outer divertor flux tube from just above the X-point to the OSP. Divertor Thomson scattering shows T_e~1 eV from the OSP up to the X-point region, with an average n_e~3x10^{20} m^{-3}. The presence of such an extended cold, dense plasma leads to significant recombination of singly-ionized carbon ions into neutral atoms as they pass from the core SOL to the divertor plate. The mean free-path (MFP) for carbon recombination approaches the divertor size, leading to significant "loss" of carbon ions before they reach the divertor plate. Therefore, one expects significant redeposition of carbon as neutral atoms. Since the neutrals are not tied to magnetic field lines and the atomic carbon MFP for ionization is much longer than the divertor scale-length (i.e. the cold plasma is transparent for the C atoms Fig. 4), a more spatially distributed redeposition pattern is expected than if carbon is only redeposited as ions. The neutral carbon flux resulting from recombination explains the presence of significant redeposition rate at the private flux region, which has ion flux that is a factor of 10 to 50 lower than seen at the strikepoints.

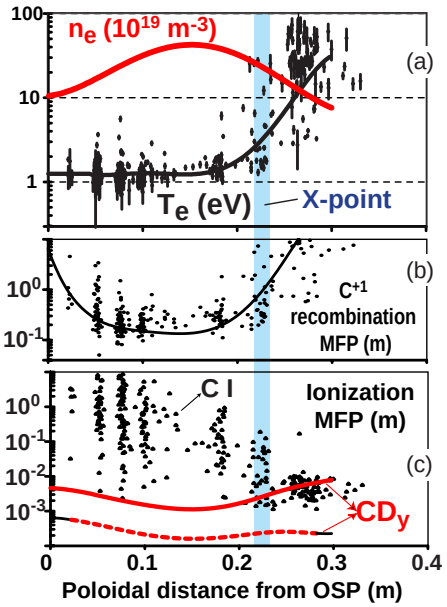

Fig. 4 Detached divertor parameters along separatrix from OSP. (a) T_e and n_e (b) C^{+1} poloidal recombination mean-free path, MFP (c) Ionization MFP for thermalized CI (points), thermal (dashed) and thermalized (solid) hydrocarbon molecules CD_y.

The influx of carbon from the main wall increases strongly with density at detachment, and is of sufficient magnitude to explain the measured deposition rate in the divertor. Fig. 5 shows the measured influx of CD, C I, and C II (C^{+1}) at the low-field side main wall. Atomic and ionic carbon particle flux are derived from the measured spectral brightness using calculated ionization per photon ratios [16]. These ratios are relatively insensitive (< factor of two) to T_e and n_e over the ranges appropriate for the midplane and divertor plasmas. Tangential and vertical views of the core plasma SOL show similar magnitudes, suggesting reasonable poloidal uniformity for the carbon influx, at least for the low-field side main wall. Also, the tangential midplane view used here is not in proximity to toroidally non-uniform surfaces (e.g bumper limiters). The main wall carbon influx increases dramatically with the increase of line-averaged density ($\Gamma_C \propto n_e^3$). A similar increase in recycling D_α light at the main wall is measured. In comparison, divertor viewing chords show little increase in carbon radiation through detachment, with the CD brightness actually decreasing.

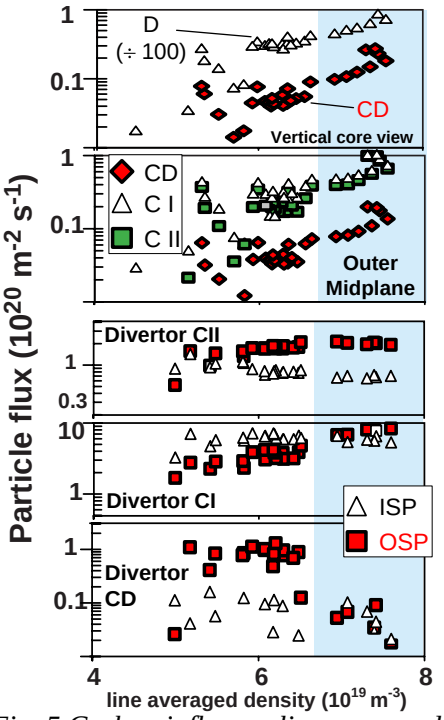

Fig. 5 Carbon influx vs. line-averaged density. Shaded region indicates OSP detachment.

At detachment, the absolute *flux* of C II is comparable at the main wall and divertor (averaging inner and outer). The implied current (particles per second) of carbon ions into the plasma is then easily dominated by the main wall, whose surface area (~50 m^2) is roughly ten times larger than the divertor surface area. Assuming poloidal and toroidal uniformity, the total incident carbon ion current from the main wall is ~ 3-5x10^{21} C s^{-1}, which is sufficient to explain the redeposition rate ~ 5 10^{20} C s^{-1} at the lower divertor. At detachment CD plays a minor role in the carbon

source for both main wall and divertor regions. The neutral C I currents are seen to be approximately equal for the main chamber and divertor, however the divertor signal likely arises from the recombination of carbon ions originating from erosion at the main wall.

4. Discussion

While net erosion is controlled by detachment, measured deposition rate ~ 3 cm/burn-year and codeposition rate > 1 kg/m^2/burn-year are unacceptable for a steady-state DT device. The stability of mm to cm thick deposits to thermal shock is likely poor, which will lead to the spontaneous spallation of such films. The formation of the redeposited films should be thought of as a gross failure of the plasma-facing component, since induced temperature excursions or particulate production could lead to macroscopic impurity influx to the core plasma. In addition, tritium uptake in these layers represents both a safety hazard and a tritium fuel cycle problem. The net divertor redeposition must arise from non-divertor erosion sources for DIII-D in the case of detachment. Main wall erosion was previously speculated as being a source of core impurities [17]. The nearly constant core carbon fraction in the absence of a significant carbon erosion source at the divertor strikepoint further supports this view (Fig. 3). We have the result that while divertor detachment succeeds in reducing or eliminating the carbon erosion source from the divertor plate, increased main wall erosion negates many of the expected improvements (such as cleaner core plasma and zero E/R in the divertor). Main wall plasma conditions and erosion must be better understood and controlled in order to take advantage of the greatly reduced sputtering in the divertor using detachment.

Acknowledgments

Work supported by U.S. Department of Energy under Contract Nos. DE-AC03-99ER54463, DE-AC05-00OR22725 and Grant No. DE-FG03-95ER54294. The originating developer of ADAS is the JET Joint Undertaking.

References

[1] Petrie, T. W., Hill, D. N., Allen, S. L., Brooks, N. H., Buchenauer, D. A. *et al*., Nucl. Fusion **37** (1997) 321.
[2] Parker, R., Janeschitz, G., Pacher, H. D., Post, D., Chiocchio, S. *et al*., J. Nucl. Mater. **241-243** (1997) 1.
[3] Wong, C. P. C., Junge, R., Phelps, R. D., Politzer, P., Puhn, F. *et al*., J. Nucl. Mater. **196-198** (1992) 871.
[4] Whyte, D. G., Coad, J. P., Franzen, P., Maier, H., Nucl. Fusion **39** (1999) 1025.
[5] Whyte, D.G., West, W.P., Doerner, R., Brooks, N.H., Isler, R.C. *et al*., "Reduction of divertor carbon sources in DIII-D," J. Nucl. Mater. (2000) accepted for publication.
[6] Fenstermacher, M. E., Allen, S. L., Brooks, N. H., Buchenauer, D. A., Carlstrom, T. N. *et al*., Phys. Plasmas **4** (1997) 1761.
[7] Brooks, J.N., Whyte, D.G., Nucl. Fusion **39** (1999) 525.
[8] Leonard, A. W., Porter, G. D., Wood, R. D., Allen, S. L., Boedo, J. *et al.*, Phys. Plasmas **5** (1998) 1736.
[9] Wampler, W.R., Bastasz, R., Whyte, D.G., Wong, C.P. C., West, W. P., J. Nucl. Mater. (2000) accepted for publication.
[10] Davis, J. W., Haasz, A. A., J. Nucl. Mater. **241-243** (1997) 37.
[11] Ehrhardt, A.B., Langer, W.D., "Collisional processes of hydrocarbons in hydrogen plasmas," Report No. PPPL-2477 (1987).
[12] Behringer, K., J. Nucl. Mater. **176-177** (1990) 606.
[13] Naujoks, D., Behrisch, R., J. Nucl. Mater. **220-222** (1995) 227.
[14] Brooks, J. N., Alman, D., Federici, G., Ruzic, D. N., Whyte, D. G., J. Nucl. Mater. **266-269** (1999) 58.
[15] Davis, J.W., Wright, P.B., Haasz, A. A., "Chemical erosion of boronized films from DIII-D tiles, " J. Nucl. Mater. (2000) accepted for publication.
[16] Summers, H.P., "Atomic Data and Analysis Structure - User Manual," Report No. JET-IR(94) (1994).
[17] Matthews, G. F., Stangeby, P. C., Elder, J. D., Gottardi, N. A. C., Harbour, P. J. *et al*., J. Nucl. Mater. **196-198** (1992) 374.